

Precision of light intensity measurement in biological optical microscopy

TYTUS BERNAS^{*†}, DAVID BARNES[#], ELIKPLIMI K. ASEM[‡],
J. PAUL ROBINSON[†] & BARTEK RAJWA[†]

^{*}Department of Plant Anatomy and Cytology, Faculty of Biology and Protection of Environment,
University of Silesia, Jagiellonska 28, Katowice, Poland

[†]Purdue University Cytometry Laboratories, 1203 S. West State St., West Lafayette, IN 47907,
U.S.A.

[#]Quantitative Imaging Corporation, 4190 Still Creek Drive, Burnaby, BC V5C 6C6, Canada

[‡]Purdue University School of Veterinary Medicine, 625 Harrison St., West Lafayette, IN 47907,
U.S.A.

Key words. CCD camera, dynamic range, fluorescence, intensity resolution, noise, photon transfer, quantitative microscopy.

Summary

Standardization and calibration of optical microscopy systems have become an important issue owing to the increasing role of biological imaging in high-content screening technology. The proper interpretation of data from high-content screening imaging experiments requires detailed information about the capabilities of the systems, including their available dynamic range, sensitivity and noise. Currently available techniques for calibration and standardization of digital microscopes commonly used in cell biology laboratories provide an estimation of stability and measurement precision (noise) of an imaging system at a single level of signal intensity. In addition, only the total noise level, not its characteristics (spectrum), is measured. We propose a novel technique for estimation of temporal variability of signal and noise in microscopic imaging. The method requires registration of a time series of images of any stationary biological specimen. The subsequent analysis involves a multi-step process, which separates monotonic, periodic and random components of every pixel intensity change in time. The technique allows simultaneous determination of dark, photonic and multiplicative components of noise present in biological measurements. Consequently, a respective confidence interval (noise level) is obtained for each level of signal. The technique is validated using test sets of biological images with known signal and noise characteristics. The method is also applied to assess

uncertainty of measurement obtained with two CCD cameras in a wide-field microscope.

Introduction

Fluorescence microscopy is an established tool in biological research. In modern biological microscopy, photomultipliers or CCD cameras generating digital images replace the human eye or photographic film as the means for fluorescence detection. Hence, instead of using relative descriptors, one can quantize fluorescence intensity in absolute (albeit arbitrary) units. Recently, efforts have been made to apply optical microscopy to obtain quantitative information on local concentration and microenvironment characteristics of biomolecules in cells and tissues (Andrews *et al.*, 2002; Lichtenstein *et al.*, 2003; Huang & Murphy, 2004; Fricker *et al.*, 2006). However, practical implementation of quantitative microscopy requires two elements. First, one has to convert fluorescence intensity to absolute units (for example, a number of molecules of interest). This task can be realized using an independent technique to provide a calibration curve (Chiu *et al.*, 2001; Sugiyama *et al.*, 2005). Alternatively, a light source of known intensity (such as LED) can be used to construct a microscope standard (Young *et al.*, 2006). Second, one has to account for the limited precision of fluorescence intensity estimation. The impact of this uncertainty (measurement error) on results of image-analysis procedures has long been recognized (Nicholson, 1978; Young, 1996; Stelzer, 1998; Zwier *et al.*, 2004; Vermolen *et al.*, 2005). Sources of uncertainty may

include the instability of a light source, optical aberrations and imperfections in alignment of elements in the optical path (Zucker, 2006a, b). Proper design and maintenance of an imaging system may eliminate or minimize these factors. However, owing to the presence of dark current and detector noise, precision of light registration in every digital microscope is limited (Jericevic *et al.*, 1989; Young, 1996; Van Den Doel *et al.*, 1998). Comprehensive characteristics for a microscope camera may be obtained using a specialized test bench (Howard, 2002; Christen *et al.*, 2005), but this approach is difficult to implement in a typical cell biology lab. The measurement precision (noise) of a digital microscope may be estimated using a standard slide made with uniformly fluorescent polystyrene beads (Zucker & Price, 2001a, b) or a piece of fluorescent plastic (Mullikin *et al.*, 1994; Van Den Doel *et al.*, 1998). Using this technique, only the total measurement noise corresponding to a single level of fluorescence intensity can be computed. Furthermore, one may not easily extrapolate the results obtained using such a simplified 'standard' sample to the conditions under which the actual biological specimens are imaged (owing to differences in emission and absorption spectra, signal intensity, refractive index, etc.).

To alleviate these problems we adapt and extend a photon-transfer technique (Janesick *et al.*, 1987; Janesick, 1997; Howard, 2002) to characterize signal and noise in fluorescence microscopic imaging. The method does not require a test bench; instead a time series of images of any stationary microscope specimen is registered. The classical photon-transfer method requires simply plotting noise as a function of signal for a small group of pixels of a CCD after being exposed to a stable, flat-field source of light. In the simplest case the total noise is estimated from the variance of the pixels. The proposed method is an extension of the photon-transfer technique in the sense that the measured quantities are based on the analysis of the variance of the detected signal. However, the source of the signal in the proposed approach is a fluorescent biological specimen, whose intensity is not stable, that is, it can change during the measurement owing to photobleaching and instability of the illumination source (e.g. a mercury lamp). Also, spatially, the source of signal is not flat, but inhomogeneous. The spatial and temporal inhomogeneity were corrected using heterogeneity measure (Amer *et al.*, 2002) and data-based mechanistic modelling of time series (Young, 1998; Young *et al.*, 1999). Consequently, the extended technique allows simultaneous determination of dark, photonic, and multiplicative components of noise under conditions of microscope imaging which closely mimic a typical biological imaging experiment. Consequently, a respective confidence interval (noise level) is obtained for each level of signal obtained from a biological sample. The technique is validated using test biological images with known signal and noise characteristics. Finally, the method is applied to assess uncertainty of an intensity measurement performed with two different CCD cameras in a wide-field microscope.

Methods

Cells and fluorescence labelling

FluoCells prepared slide #2 (Molecular Probes) was used in all experiments. The slide contained fixed bovine pulmonary artery endothelial cells in which microtubules were labelled using mouse anti-bovine α -tubulin monoclonal antibodies in conjunction with BODIPY FL goat anti-mouse IgG antibody; the cell nuclei were labelled with DAPI.

Microscope imaging

Images of the endothelial cells were registered using a Nikon E1000 wide-field fluorescence microscope. The microscope was equipped with a Nikon 40 \times Fluor oil-immersion objective lens (NA 1.3) and a 100-W Hg arc lamp. The BODIPY FL fluorescence was registered using a 475- to 495-nm excitation filter (band pass), a 505-nm long-pass dichroic mirror and a 525- to 565-nm emission filter (band pass). Two monochromatic CCD cameras (Qimaging, Burnaby, Canada) were used for image registration: a Rollera XR and a Retiga 4000R. Specifications for the cameras are summarized in Table 1.

Neutral density filters were used to attenuate the flux of excitation light: 128 \times (16 \times +8 \times) with the Rollera XR and 16 \times with the Retiga 4000R. The microscope aperture diaphragm was fully open, whereas the field diaphragm was adjusted to match the field of view of the objective. Image collection was carried out at room temperature. The cameras were cooled to 25 $^{\circ}$ C below ambient.

Time series of 128 images of stationary (fixed) cells were collected using full frame (no binning) at 5-s intervals. The series were registered for each of the cameras operating at three gain settings and for 0.25- or 0.75-s acquisition times. Image acquisition was controlled using ImagePro Plus v 5.1 (Media Cybernetics, Silver Spring, Maryland).

Decomposition of pixel intensity changes

The source of signal used in our system is spatially and temporarily inhomogeneous. The traditional method

Table 1. Specifications of CCD cameras.

Camera	Retiga 4000R	Rollera XR
Chip type (manufacturer)	KAI-4021 (Kodak)	VQE3618L (proprietary)
Chip size (pixels)	2048 \times 2048	696 \times 520
Pixel size (μ m)	7.4 \times 7.4	13.7 \times 13.7
Pixel area (μ m ²)	54.76	187.69
Full well capacity (e ⁻)	40.000	22.000
Dark current (e ⁻ /pixel/s)	1.64 (cooled)	1.78 (non-cooled)
Readout noise (e ⁻)	12	10
Quant. eff. at 545 nm	45%	70%

of measuring the photon transfer-curve requires the CCD detector to be exposed to a uniform and stable illumination field. As the spatial and temporal uniformity decreases, it becomes essentially impossible to approximate a photon-transfer curve using standard techniques. Therefore the first step in our method requires spatial and temporal decomposition of the collected images using the unobserved components methodology.

The fluorescence intensity changes in time were modelled (separately for every image pixel) using three components: a systematic trend (related to photobleaching), a periodic component (associated with fluctuation of the excitation light source) and an irregular component (which represents noise). Following (Young, 1998) we can study our system using a simple univariate version of the unobserved components model: $y_t = T_t + S_t + e_t$, where t denotes the value of the associated pixel intensity at the t th time point, y is the observed value, T is a trend (or low frequency component), S is a periodic (or 'seasonal' component) and e is an irregular component. All the calculations were executed on a pixel-by-pixel basis utilizing the CAPTAIN modelling toolkit (Young, 1998). First, the stochastic trend component was estimated using the integrated random walk (IRW) model:

$$\begin{aligned} I_t &= T_t + e_t \\ T_t &= 2T_{t-1} - T_{t-2} + \eta_t \end{aligned} \quad (1)$$

where I_t is registered fluorescence intensity (at t th time point), T_t is the smoothed intensity at t th time point, T_{t-1} and T_{t-2} are values of T_t at two previous time points, e_t is measurement noise (zero mean, variance σ_e^2) and η_t is the system disturbance (zero mean, variance σ_η^2).

The ratio of variances corresponding to the system disturbance and the measurement noise (noise variance ratio, NVR, σ_η^2/σ_e^2) was set to 10^{-4} . This value was chosen empirically so that the T_t represented the components corresponding to time period larger than 64 samples (280 s) but excluded components corresponding to shorter periods. The instantaneous values of e_t and η_t were fitted (using least linear squares) so as to minimize difference between T_t and I_t at the set NVR. Hence T_t represented a systematic trend associated with photobleaching of biological samples. The trend was subtracted from the observed intensity (I_t). The de-trended data were used to isolate periodic components of intensity changes (corresponding to periods smaller than 64 samples – 280 s) with the dynamic harmonic regression (DHR):

$$\begin{aligned} I_t^d &= \sum_{j=0}^{s/2} [a_{jt} \cos(\omega_j t) + b_{jt} \sin(\omega_j t)] + e_t \\ \omega_j &= \frac{2\pi j}{s}, \quad a_{jt} = a_{j,t-1} + \eta_t, \quad b_{jt} = b_{j,t-1} + \eta_t, \end{aligned} \quad (2)$$

where s is the maximum order of the periodic component, I_t^d is detrended fluorescence intensity, e_t is measurement noise and η_t is system disturbance.

The DHR model is an extension of classical Fourier analysis with the number of frequencies limited by the number of observations. The optimal order of DHR (number of significant periodic components, $s/2$) was estimated using the Akaike Information Criterion (AIC) (Akaike, 1974, 1981). The AIC is a measure of the goodness of fit of an estimated statistical model. Since the AIC also includes a penalty, which increases with the number of estimated parameters, it discourages overfitting. Subsequently, the IRW (Eq. 1) and optimal order DHR (Eq. 2) were used jointly to fit the trend and periodic component to the initial fluorescence intensity data (I_t). One should note that NVR was optimized in this step as well to minimize residual variance globally. The sum of the trend and periodic components represented the true instantaneous fluorescence intensity (signal, S_t^i) at every time point. Hence, the instrumental noise (for a pixel at a given time point) and its variance (for a signal level) were:

$$N_t^i = |S_t^i - I_t^i|, \quad V_{S=F} = \frac{\sum_{i,t} \delta_{SF} (N_t^i)^2}{\sum_{i,t} \delta_{SF}}, \quad (3)$$

where N is the noise, S is the signal, I is registered fluorescence intensity at i th and t th points of the image time series, $V_{S=F}$ is variance of the signal at F th level.

The estimates of other two components of time series (periodic component and trend) can be further used to characterize the stability of the light source and the photobleaching rate of the fluorochromes used in the experiment. However, they were utilized here only to provide an estimate of total signal level (fluorescence and background) and thus to calculate the corresponding level of total noise.

Calculation of noise levels and background signal

In order to estimate the background signal, uniform dark image regions were identified for each time series. These regions (represented using binary masks) comprised pixels characterized by fluorescence intensity and local fluorescence heterogeneity that were smaller than 10% of their respective maxima. The heterogeneity was measured using the algorithm described in (Amer *et al.*, 2002). Briefly, eight directional high-pass filters were applied to an image and resulting images were added. 10% of pixels having the smallest sums were chosen to represent the most homogenous image regions. Average intensity (I_b) calculated in dim and homogenous regions was taken as the background (i.e. pixel value of an image registered in the absence of fluorescence). The noise variance (V , Eq. 3) was plotted against the signal corrected for background ($S_c = S - I_b$). A quadratic function was fitted to these data in order to characterize signal-noise dependency:

$$V = A + P S_c + M S_c^2, \quad (4)$$

where M , P and A are estimators of the signal variance associated with the multiplicative, Poisson (photonic) and

additive noise components. The standard deviation of I_b (\sqrt{B}) was calculated to estimate background noise.

Algorithm validation

A time series of 128 images of fluorescent endothelial cells was registered (0.750-s acquisition time) as described in the previous paragraphs. A time-averaged image was calculated and subjected to filtering with hybrid median (3×3 kernel). The background value was set to 0 and the processed image was used as a template for generation of synthetic test images. Series of 128 test images were generated by addition to the template of various amounts of additive and Poisson noise and background intensity. Noise and background levels were calculated from the test series using the algorithm described in the previous paragraphs. Estimated parameters were plotted against their true counterparts.

Calculation of significant intensity levels and photon equivalence units

Owing to the presence of noise in the images, not all intensity differences can be considered significant. Thus, the number of meaningful intensity levels is lower than the nominal dynamic range provided by the cameras (12 bits, 4096 levels). Hence, the significant levels were calculated iteratively using the following algorithm (see the Appendix):

1. Input I_b , A , P , M (Eq. 4),
2. Set $k = 0$,
3. **Do:**
 4. Set $k = k + 1$,
 5. Set $I_{\text{med}}^k = I_b$,
 6. Set $\sigma(I_{\text{med}}^k) = \sqrt{A + I_{\text{med}}^k \cdot P + (I_{\text{med}}^k)^2 \cdot M}$,
 7. Set $I_{\text{high}}^k = I_{\text{med}}^k + 1.96 \cdot \sigma(I_{\text{med}}^k)$,
 8. Set $I_{\text{low}}^{k+1} = I_{\text{high}}^k$,
 9. Calculate I_{med}^{k+1} so that $I_{\text{med}}^{k+1} - I_{\text{low}}^{k+1} = 1.96 \sigma \cdot (I_{\text{med}}^{k+1})$,
4. **Loop while** $I_{\text{med}}^{k+1} < 4095$
5. Terminate & output vectors I & k .

The algorithm produces a set of I_{med}^k for which $I_{\text{med}}^k - I_{\text{med}}^{k-1} = 1.96[\sigma(I_{\text{med}}^k) + \sigma(I_{\text{med}}^{k-1})]$. The I_{med}^k values smaller than I_{max} represent intensity levels significantly different from one another with probability of 0.95, which corresponds to 95% confidence in the sense of Student's t test (hence the 1.96 factor). The choice of confidence interval was arbitrary. However, similar calculations can be performed for every confidence level. The set of values was used to segment the representative images by setting all pixel intensities (I_r) to the nearest significant level. A periodic lookup table was used in order to visualize clearly numerous intensity levels (which corresponded to pixel-to-pixel intensity differences) in

raw data and few intensity levels which were significant in processed data. If a non-periodic lookup table (256 colours) with continuous tone transition (similar to that used in Fig. 6) was employed pixels of similar intensities (values) would be represented by almost identical colour. Results of such operation would be equivalent to reduction of number of intensity levels performed in an arbitrary manner (as opposed to strategy based on statistical model and described earlier in this section). The two CCD cameras used differed with respect to photon noise level (represented by P coefficient in the Eq. 4) and registered signal intensity (which depended on the excitation light flux). Therefore the pixel intensity in the images was scaled by:

$$I_s = S_c \frac{E_f}{E_{f0} \sqrt{P}}, \quad (5)$$

where S_c is background-corrected signal, E_{f0} is the attenuation factor of the neutral density excitation filter used with Rollera XR (128) and E_f is the respective attenuation factor for Rollera XR or Retiga 4000R.

The scaled intensity (I_s) represents the situation in which one digital unit corresponds to one detected photon under similar imaging conditions, which comprise the same fluorescence excitation flux, identical camera settings (gain, acquisition time and offset) and similar specimen (fluorescently labelled cell from the same population). A non-periodic continuous tone (from red through green to blue) lookup table was used to represent intensity in scaled images.

Results

Algorithm validation

A test set containing a series of synthetic images generated by addition of defined amounts of Poisson noise, additive noise and background signal (see Materials and Methods) was subjected to the proposed noise-analysis procedure. The estimated values of these noise parameters were plotted against the respective true values (Fig. 1) in order to estimate accuracy of the algorithm. The Poisson noise levels were estimated precisely and accurately (Fig. 1A). Lower precision was obtained for additive noise (Fig. 1B) and background intensity (Fig. 1C). These two parameters were estimated accurately in all cases but one. When additive noise ($\sigma = 33.3$) was present and background intensity was set to 0 (arrow in Fig. 1), underestimation of the former and overestimation of the latter occurred. However, such a situation is unlikely to be encountered if microscope imaging is performed correctly (as discussed further). Furthermore, no multiplicative noise was present and the estimated coefficients for this type of noise (Eq. 4) were below 0.001 ± 0.0001 (data not shown). Hence, it may be concluded that the proposed algorithm renders accurate estimations of the Poisson noise, additive noise and background signal.

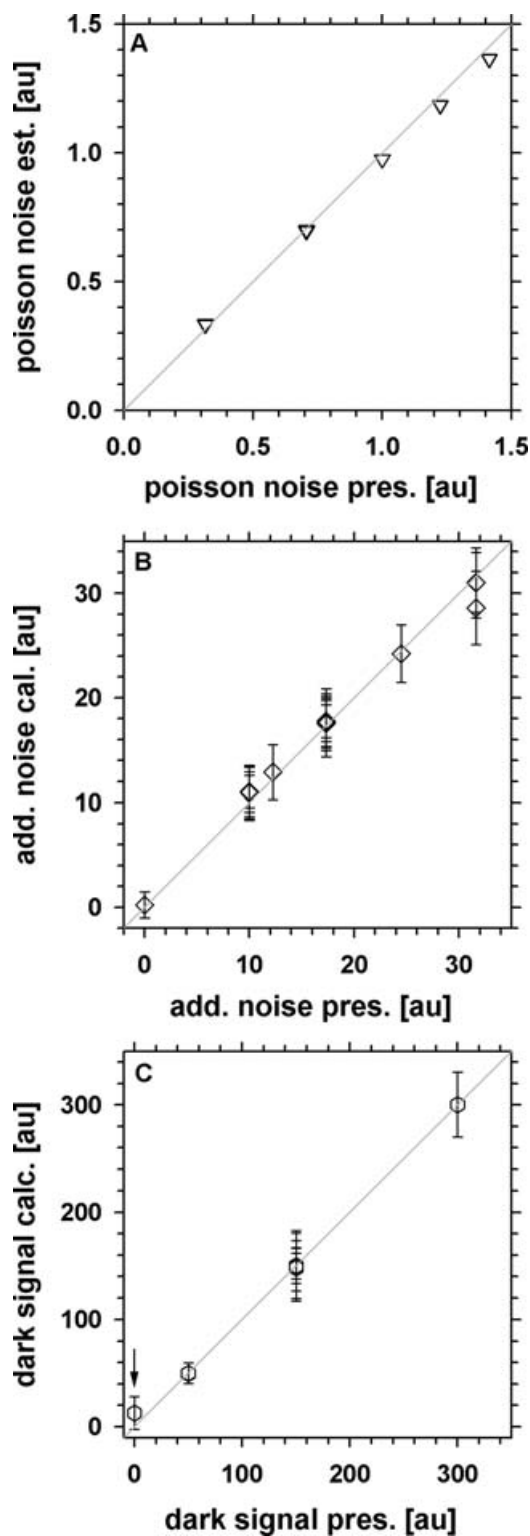


Fig. 1. Accuracy of the noise estimation algorithm. Estimated levels of the Poisson noise (A), additive noise (B) and dark signal (C) are plotted against true levels of these parameters. Standard deviations are indicated with error bars. Arrow indicates a case when additive noise ($\sigma = 33.3$) was present and background was set to 0.

CCD test

Poisson noise. Square roots of Poisson noise coefficients (Eq. 4) were plotted against the respective values of gain of the two CCD cameras (Fig. 2). The amount of this type of noise depended linearly on the gain for the Retiga 4000R (Fig. 2, triangles up) and the Rollera XR (Fig. 2, squares). This dependence was

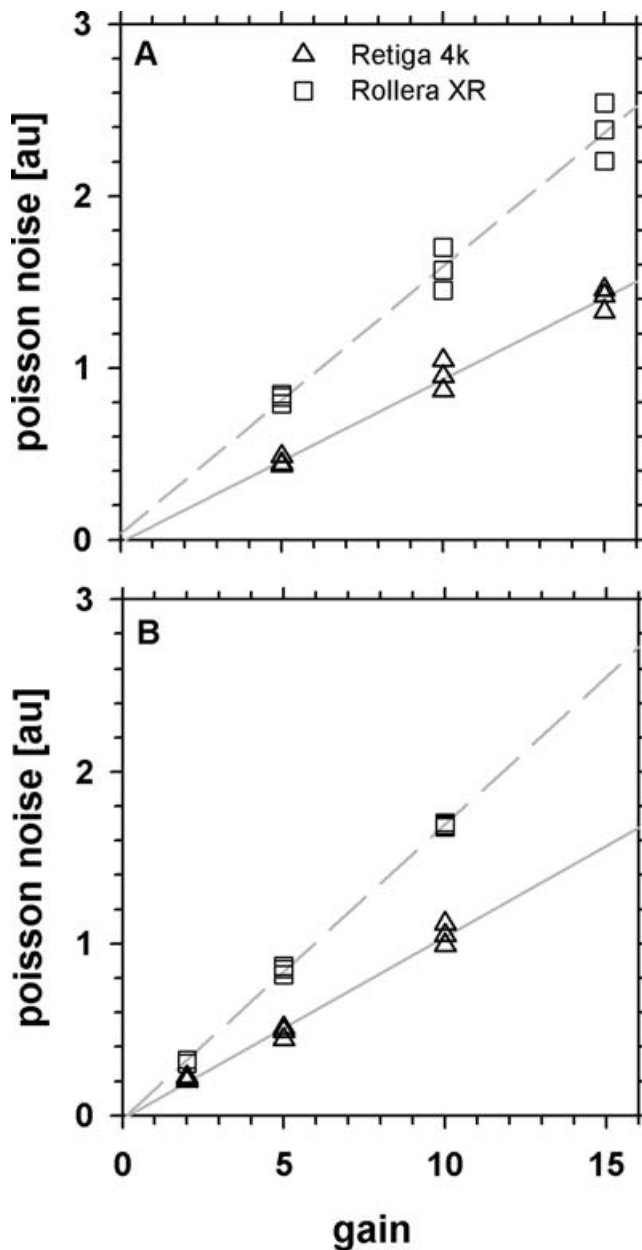


Fig. 2. Poisson noise of CCD cameras. Square roots of the respective fit coefficients (\sqrt{P} , Eq. 4) are plotted against the gain of the Retiga 4000R (triangles up) and the Rollera XR (squares). The noise was measured at 0.250-s (A) and 0.750-s (B) image acquisition times. Fitted linear functions are represented with lines: solid (Retiga 4000R) and long dash (Rollera XR).

Table 2. Dependence of Poisson noise on CCD gain.

	Acq. Time (s)	Slope (SL_p)	Intercept (IN_p)	Correlation (r^2)
Retiga 4000R	0.250	0.0948 ± 0.007	-0.028 ± 0.005	0.98
	0.750	0.0986 ± 0.006	-0.018 ± 0.002	0.99
Rollera XR	0.250	0.1521 ± 0.012	0.059 ± 0.009	0.98
	0.750	0.1731 ± 0.023	-0.027 ± 0.003	0.99

The coefficients of the fitted linear functions ($P = SL_p \times \text{gain} + IN_p$) from Fig. 2A (0.250 s) and Fig. 2B are given with their standard errors.

not affected by acquisition time (compare Figs 2A and B, see Table 2) or offset. One should note that the noise approached 0 with decreasing gain, which indicates that this parameter depended only on the signal (amount of detected light). On the other hand, the two cameras differed with respect to the increase of the Poisson noise with gain (Table 2). As a result a higher amount of this form of noise was present in the images registered with the Rollera XR than in images registered with the Retiga 4000R.

Additive noise. Square roots of additive noise coefficients (Eq. 4) were plotted against the respective values of gain of the two CCD cameras (Fig. 3). Like Poisson noise, the amount of additive noise depended linearly on the gain for the Retiga

4000R (Fig. 3, triangles up) and the Rollera XR (Fig. 3, squares). This dependence was not affected by the offset and acquisition time (compare Figs 3A and B, see Table 3). A small residue of additive noise was predicted at the gain of 0 (Table 3). This value was close to the difference between the additive (\sqrt{A}) noise and (\sqrt{B}) background noise (Figs 3C and D). Hence both these parameters may be regarded as estimators of the dark noise. One may note that images registered with the Rollera XR contained more dark noise than images registered with the Retiga 4000R.

Background signal. Mean values of background signal (see Materials and Methods) were plotted against the offset (Fig. 4). The background signal increased with acquisition

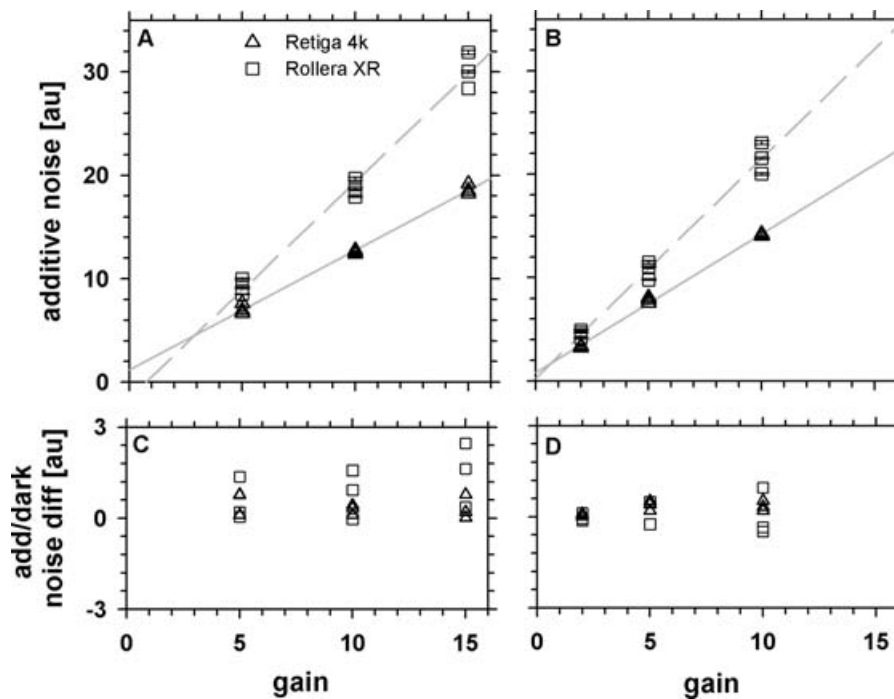


Fig. 3. Additive noise of CCD cameras. Square roots of the respective fit coefficients (\sqrt{A} , Eq. 4) are plotted against the gain of the Retiga 4000R (triangles up) and the Rollera XR (squares). The noise was measured at 0.250-s (A) and 0.750-s (B) image acquisition times. Fitted linear functions are represented with lines: solid (Retiga 4000R) and long dash (Rollera XR). The respective differences between the additive noise (\sqrt{A} , Eq. 4) and the background noise (\sqrt{B}) of the Retiga 4000R (triangles up) and the Rollera XR (squares) measured at 0.250-s (C) and 0.750-s (D) acquisition times are plotted against the gain as well.

Table 3. Dependence of additive noise on CCD gain.

	Acq. Time (s)	Slope (SL_a)	Intercept (IN_a)	Correlation (r^2)
Retiga 4000R	0.250	1.148 ± 0.101	1.25 ± 0.79	0.99
	0.750	1.394 ± 0.092	0.56 ± 0.03	0.99
Rollera XR	0.250	2.030 ± 0.150	-1.07 ± 0.10	0.98
	0.750	2.087 ± 0.371	-0.37 ± 0.22	0.99

The coefficients of the fitted linear functions ($A = SL_a \times \text{gain} + IN_a$) from Fig. 3A (0.250 s) and Fig. 3B are given with their standard errors.

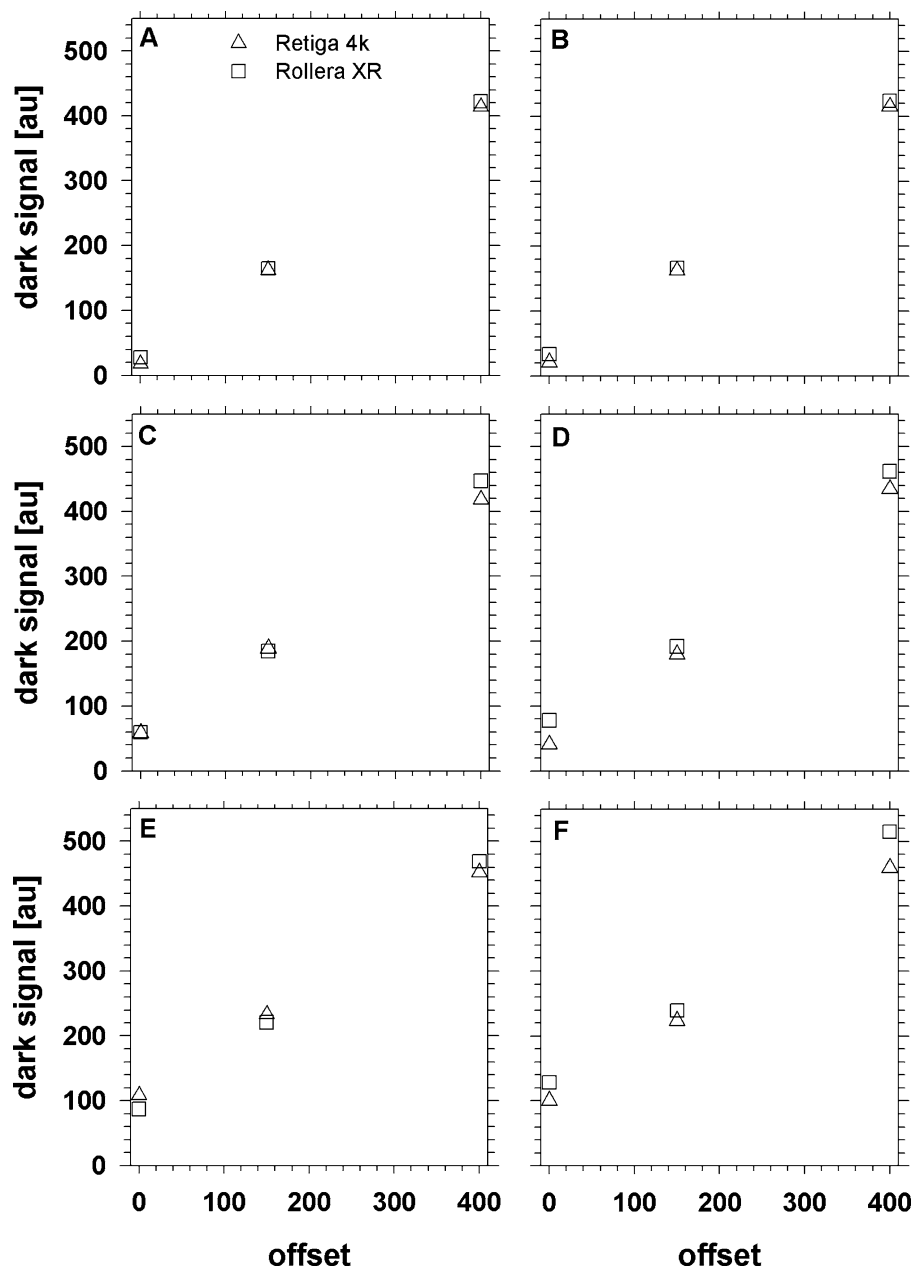


Fig. 4. Background signal of CCD cameras. The intensity (I_b , digital units) was plotted against the offset of the Retiga 4000R (triangles up) and the Rollera XR (squares). The background was measured at 0.250-s (A, C, E) and 0.750-s (B, D, F) image acquisition times. The gain of the cameras was set to 2 (B), 5 (A, D), 10 (C, F) or 15 (E).

Table 4. Significant ($p = 0.95$) intensity levels of CCDs with the corresponding (minimal) number of bits needed to code these levels.

	Acq. Time (s)	Gain	Offset (AU)					
			0		150		400	
			Levels	Bits	Levels	Bits	Levels	Bits
Retiga 4000R	0.250	5	74	7	72	7	70	7
		10	36	6	36	6	34	6
		15	24	5	24	5	23 ⁺	5
	0.750	2	190*	8	186	8	178	8
		5	74	7	72	7	69	7
		10	36	6	36	6	34	6
Rollera XR	0.250	5	49	6	48	6	47	6
		10	24	5	23	5	23	5
		15	15	4	15	4	15	4
	0.750	2	84*	7	81	7	78	7
		5	36	6	35	6	34	6
		10	20	5	19	5	18 ⁺	5

The highest obtained numbers of levels are indicated with asterisks, the lowest with crosses.

time (compare Figs 4A, C and E with Figs 4B, D and F) and gain (compare Figs 4A and B, C and D and E and F) for the two CCDs. A linear increase of the background signal with the offset was detected as well. It should be noted that the two CCDs exhibited similar levels of background signal.

Practical applications

Calculation of practical dynamic range. The two cameras registered images with 4096 nominal intensity levels (12-bit digitization). However, owing to the presence of noise not all differences in intensity between pixels may be considered significant (see Materials and Methods), and consequently practical dynamic resolution is lower than nominal. Hence, the number of significant intensity levels (with 0.95 probabilities) was calculated at several values of CCD settings (gain, acquisition time and offset) and are presented in Table 4.

The number of significant levels decreased conspicuously with increasing gain of the two CCDs. Furthermore, a moderate reduction of practical dynamic range was observed when the offset was increased. Increase of acquisition time did not significantly affect the number of levels for the Retiga 4000R. However, a decrease in the practical dynamic range occurred in the Rollera XR at longer acquisition times. In general, higher practical dynamic range was obtained with the Retiga 4000R than with the Rollera XR. In order to illustrate this notion, representative images were segmented (see Materials and Methods) and displayed with significant intensity levels only (Fig. 5).

Estimation of equivalent number of detected photons. One should note that the cameras operated at different fluxes

of excitation light and therefore different levels of emitted fluorescence. Hence the number of equivalent detected photons was estimated from the Poisson noise and the images were normalized to represent similar excitation intensities (see Materials and Methods). One should note that these figures represent situation in which both detectors operate as ideal photon counters. The scaled representative images (Fig. 6) demonstrate that under similar imaging conditions one may expect significantly higher number of detected photons (approximately $2.5\times$) per pixel with the Rollera XR (Figs 6A and C) than with the Retiga 4000R (Figs 6B and D).

Discussion and conclusions

Quantitative microscopy requires knowledge about the precision of light detection. Comprehensive characteristics of detector performance can be obtained from a microscope, with specialized test benches (Christen *et al.*, 2005; Howard, 2002). The proposed technique provides less detailed results but uses a time series of images of a real biological specimen. Hence, it can be implemented in any biological microscopy lab to test the precision of light intensity measurement obtained from any fluorescence microscope. Noise estimation in the proposed technique is performed in a manner similar to the photon-transfer curve method (Janesick, 1997; Howard, 2002; Christen *et al.*, 2005; Kinney & Talbot, 2006). However, in the proposed technique, estimation of background is executed separately, which eliminates manual segmentation of the photon-transfer curve (Howard, 2002; Kinney & Talbot, 2006). Moreover, signal estimation is carried by decomposing the intensity change in time on a pixel-by-pixel

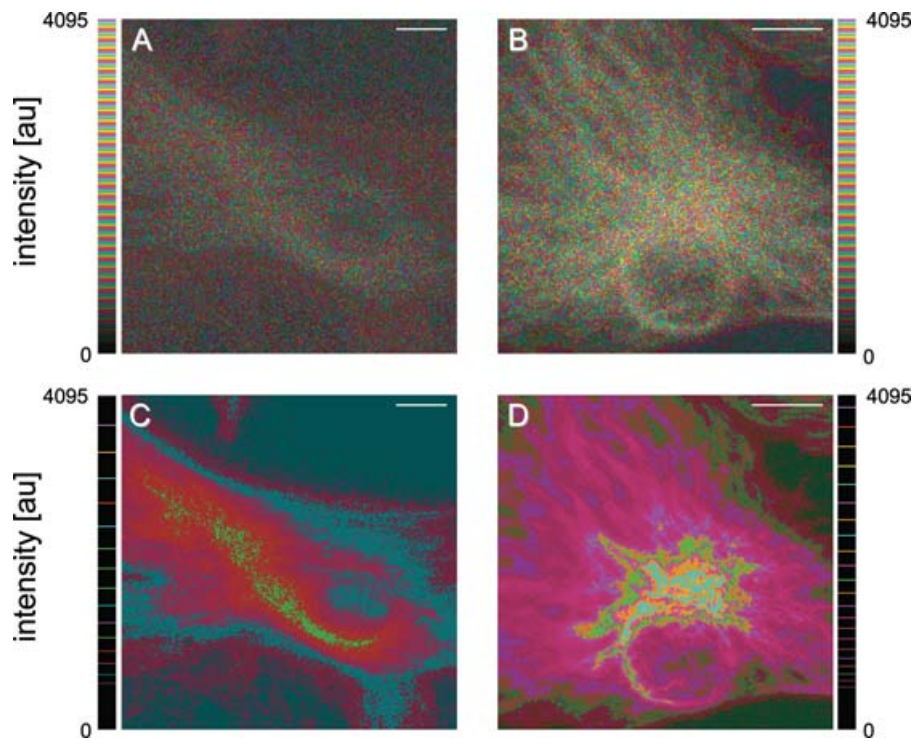


Fig. 5. Significant ($p = 0.95$) intensity levels in the images registered with the Retiga 4000R (A, C) and the Rollera XR (B, D). Raw images (A, B) were segmented (C, D) to represent the intensity levels with 95% confidence (see Materials and Methods). The images were multiplied by 1.078 so that the brighter of the two (A, C) occupy whole intensity scale. The segmented images are shown in pseudo-colour using a periodic lookup table (see Materials and Methods). Scale bar $10 \mu\text{m}$.

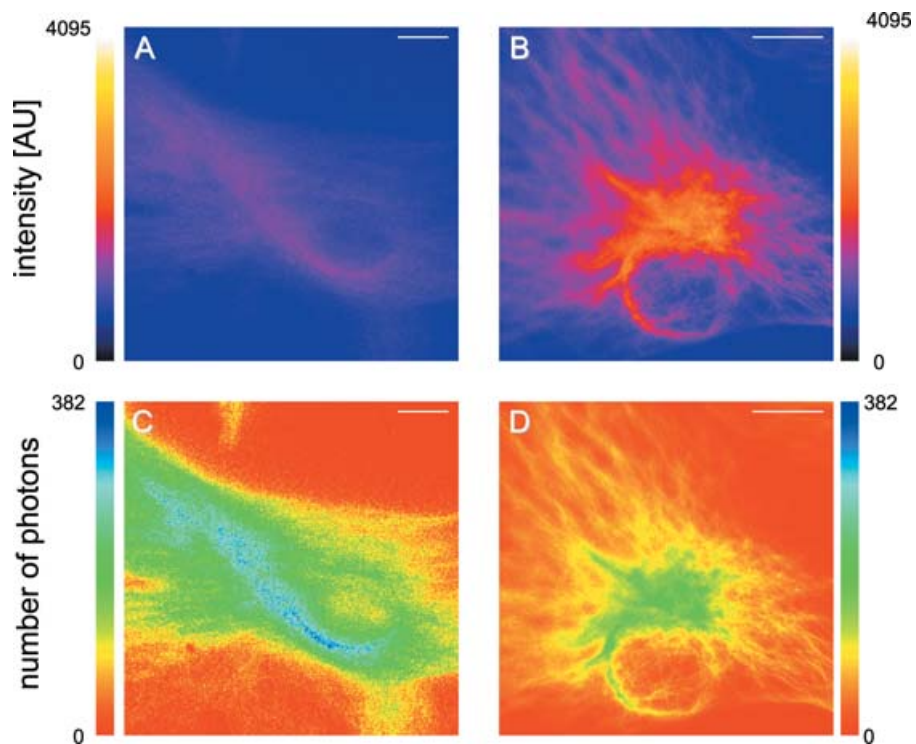


Fig. 6. Numbers of equivalent photons in the images registered with the Retiga 4000R (A, C) and the Rollera XR (B, D). The images are scaled (see Materials and Methods) and presented in pseudo-colour using a continuous tone non-periodic lookup table (see Materials and Methods). Scale bar $10 \mu\text{m}$.

basis instead of by calculating a simple average over a set of image pixels (Janesick, 1997; Howard, 2002) or time points (Howard, 2002; Kinney & Talbot, 2006). The presented data were processed using an IRW/DHR modelling approach, but most likely similar results could have been obtained utilizing other methods of time series decomposition and forecasting such as ARIMA (autoregressive integrated moving average). One may generate a photon-transfer curve in a simpler way using a locally uniform fluorescent specimen (i.e. one in which different regions correspond to different fluorescence intensity) like a partially defocused slide. However, this technique would require spatial fluorescence distribution to be fully characterized (in order to segment the uniform regions correctly). The proposed technique is designed for non-uniform specimens but does not require any prior knowledge about spatial fluorescence distribution. Moreover, temporal invariability of the registered luminescence is not a prerequisite for application of this method. Hence, the technique may be used with biological specimens, which typically exhibit spatially and temporally heterogeneous fluorescence. Furthermore, the specimens may be imaged under non-ideal (realistic) conditions which involve photobleaching of fluorescent labels (Song *et al.*, 1995; Van Oostveldt *et al.*, 1998; Kunz & MacRobert, 2002; Bernas *et al.*, 2004) and instability of illumination source (Zucker & Price, 2001b).

One should note that the algorithm required a stationary biological specimen to register image time series. Therefore, presence of axial (z) or lateral (xy) specimen drift might impair accuracy of the presented method as it might contribute to pixel intensity variation. In our experience total lateral (xy) displacement (stage drift) as high as $1\ \mu\text{m}$ per an image time series did not alter the values of additive and Poisson by more than 1%. Similarly, axial drift up to $0.5\ \mu\text{m}$ did not significantly affect the performance of the algorithm. However, no systematic studies were carried out and the images were not corrected for drift. Instead care was taken to avoid axial and lateral drift by maintaining constant room temperature and eliminating airflow. As a result, possible drift in the presented experiments (10 min) did not exceed the indicated values.

The presented implementation used data from 128 images registered at 5-s intervals. Hence one might capture periodic components characterized by period of 10s or higher (according to the Nyquist criterion). On the other hand, the systematic trend, which corresponded to photobleaching of BODIPY, might be determined accurately if the specimen were illuminated for 10 min. Furthermore, when 128 images were registered one might expect typically 2000 data points (on average) corresponding to each signal level (of 4096), even with a camera equipped with a small CCD chip (VQE3618L, 696×520 pixels). Therefore, a photon-transfer curve could be determined in a reliable manner by simple least linear squares fitting in our imaging conditions. Nonetheless, with different conditions (slower photobleaching kinetics, better

illumination stability etc.) a smaller number of images and a shorter registration time might give similar accuracy. Hence, one may optimize data-registration conditions if some information on stability of fluorescent probes and of the imaging system is available.

The algorithm provided accurate estimation of multiplicative noise, Poisson noise, additive noise and dark current in an orthogonal manner (independently of one another). Errors occurred only when additive noise was present and background intensity was set to 0. One should note that since the images contained only non-negative values the actual distribution of additive noise was not symmetric, which increased the apparent background intensity and consequently introduced bias in the calculation of Poisson noise. One should note that such a situation is unlikely if the detector offset is adjusted correctly, so that the registered image contains no zeros.

The validated algorithm was applied to characterize performance of two CCD cameras often used in our laboratory for biological fluorescence microscopy. Images registered using the Retiga 4000R exhibited the lowest level of Poisson noise per pixel. The level of Poisson noise in the Rollera XR was approximately 1.80 times higher than in the Retiga 4000R (at any gain). Levels of this type of noise are proportional to the square root of the number of detected photons. One may note that these ratios correspond well with the square roots of ratios of respective pixel areas (1.85, see Table 1). On the other hand one might expect a higher number of registered photons (per unit of light-sensitive pixel area) in the Rollera XR than in the Retiga 4000R owing to the difference in quantum efficiency. One should note that levels of background noise (\sqrt{B}) and additive noise (\sqrt{A}) were similar in all the cameras tested. Thus, the variability in the background signal may account for all the noise that is independent on the fluorescence intensity. All the tested cameras exhibited similar mean values of the background signal (I_b). However the level of additive noise was approximately 1.61 times higher in the Rollera XR than in the Retiga 4000R. This value is lower than square root of the ratios of respective pixel areas. One may expect the background noise to be proportional to the square root of the pixel size. Conversely, the nominal dark current of the Rollera XR was lower than that of the Retiga 4000R (see Table 1).

Output of the proposed algorithm was used to estimate the practical intensity resolution (dynamic range) of cameras used to perform biological imaging. Owing to the presence of noise, the significant difference in intensity is usually greater than one intensity unit. Consequently the maximum number of significant intensity levels is lower than expected from the specifications (12-bit, 4095 levels). One may note that the total noise level of the Rollera XR was higher than that of the Retiga 4000R. Consequently the highest available dynamic resolution of the Rollera XR is lower than that of the Retiga 4000R. On the other hand, the number of registered photons (per pixel) may be expected to be higher in the former

than in the latter. This notion is confirmed by the fact that the scaled images registered with the former camera were brighter than those registered with the latter device. Therefore, under similar imaging conditions one may expect that the number of populated significant intensity levels will be higher with the Rollera XR than in the Retiga 4000R.

The described test can be performed with any CCD cameras used for fluorescence imaging, in order to establish optimal imaging conditions for a given type of biological specimen. One may note that at low levels of emitted fluorescence (fewer than 100 photons reaching detector pixel) the intensity resolution of a typical CCD is determined primarily by additive noise, which comprises spurious, dark and readout noise components. On the other hand, the number of populated intensity levels depends on detector sensitivity, which is determined by quantum efficiency and gain. Therefore, at low levels of fluorescence, EMCCDs and ICCDs, despite high dark and amplification noise, are likely to outperform conventional CCDs owing to their high gain. However, at higher levels of fluorescence (more than 100 photons per pixel), where the noise is dominated by the photonic component, the presence of amplification noise (i.e. noise factor higher than 1) in EMCCDs and ICCDs may render performance of these detector inferior to that of conventional CCDs. Using the presented algorithm one may verify these theoretical predictions for a given imaging system.

Detailed information on practically available intensity resolution of cameras makes it possible to compare intensities in different image regions in a statistically meaningful manner. Moreover, using error propagation theory one may perform a similar estimation for every combination of pixels. In other words, one may assign confidence intervals to every parameter derived from image-analysis procedures. Therefore, using the proposed technique one may estimate the true biological (cell-to-cell) variability with respect to image-derived measures. This is an important consequence of the proposed technique, and to our knowledge, previously proposed calibration methods do not provide such a capability.

One may postulate that non-specific fluorescence (background) limits accuracy of measurement of specific fluorescence in biological specimens to a greater degree than does instrument noise. It should be noted that the presence of non-specific fluorescence may impede accurate detection of specific signals owing to two effects. First, non-uniform, non-specific fluorescence (background) may obscure distribution of specific fluorescence. Second, non-specific fluorescence increases the total amount of photon noise, thus reducing the SNR of specific fluorescence. Non-specific background has to be characterized using an appropriate control in a separate experiment. The presented method makes it possible to estimate the contribution of such background to the SNR of specific fluorescence.

The analysis of fluorescence intensity in time yields systematic component of the intensity changes as one of

the algorithm outputs. This information may be used not only to estimate instantaneous fluorescence signal but also to reconstruct kinetics photobleaching. Characteristics of photobleaching kinetics may be applied to optimize imaging conditions and to restore faded images (Bernas *et al.*, 2004). One may also use photobleaching to correct non-uniform microscope illumination (Van Den Doel *et al.*, 1998; Zwier *et al.*, 2004) to resolve fluorochromes with similar spectral properties (Brakenhoff *et al.*, 1994) or to standardize excitation intensity in a fluorescence microscope (Zwier *et al.*, 2004).

Another consequence of the performed statistical intensity analysis is the fact that segmentation with respect to the statistically significant levels produces images characterized by only a few intensity values. As a result, these images with sparse histograms may be represented using fewer bits than required by nominal intensity resolution. Hence one may postulate that efficient compression of the images may be obtained using histogram-packing techniques based on the proposed approach (Starosolski, 2005).

Acknowledgments

This work was supported by Foundation for Polish Science (HOM/02/2007 grant to TB). We acknowledge excellent technical assistance by Gretchen Lawler, MSc.

References

- Akaike, H. (1974) A new look at the statistical model identification. *IEEE Trans. Auto. Contr.* **19**(6), 716–723.
- Akaike, H. (1981) Likelihood of a Model and Information Criteria. *J. Econometrics* **16**, 3–14.
- Amer, A., Dubois, E. & Mitiche A. (2002) Reliable and fast structure-oriented video noise estimation. *Proc. IEEE Int. Conf. On Image Processing* **1**, 840–843.
- Andrews, P.D., Harper, I.S. & Swedlow, J.R. (2002) To 5D and beyond: quantitative fluorescence microscopy in the postgenomic era. *Traffic* **3**(1), 29–36.
- Bernas, T., Zarebski, M., Cook, P.R. & Dobrucki, J.W. (2004) Minimizing photobleaching during confocal microscopy of fluorescent probes bound to chromatin: role of anoxia and photon flux. *J. Microsc.* **215**, 281–296.
- Brakenhoff, G.J., Visscher, K. & Gijsbers, E.J. (1994) Fluorescence bleach rate imaging. *J. Microsc.* **175**, 154–161.
- Chiu, C.S., Kartalov, E., Unger, M., Quake, S. & Lester, H.A. (2001) Single-molecule measurements calibrate green fluorescent protein surface densities on transparent beads for use with 'knock-in' animals and other expression systems. *J. Neurosci. Methods* **105**(1), 55–63.
- Christen, F., Kuijken, K., Baade, D., Cavadore, C., Deiries, S. & Iwert, O. (2005) Fast Conversion Factor (Gain) Measurement Of A CCD Using Images With Vertical Gradient. *Proceedings of the Scientific Devices Workshop*, Taormina, Italy.
- Fricker, M., Runions, J. & Moore, I. (2006) Quantitative fluorescence microscopy: from art to science. *Annu. Rev. Plant. Biol.* **57**, 79–107.
- Howard, N.E. (2002) Photon Transfer Technique. *OpSci Application Note OAN-006, OPSCI* (<http://www.opsci.com>).

- Huang, K. & Murphy, R.F. (2004) From quantitative microscopy to automated image understanding. *J. Biomed. Opt.* **9**(5), 893–912.
- Janesick, J.R. (1997) CCD transfer method: standard for absolute performance of CCDs and digital CCD camera systems. *Proc. SPIE.* **3019**, pp. 70–102.
- Janesick, J., Klaasen, K. & Elliott, T. (1987) CCD charge collection efficiency and the photon transfer technique. *Opt. Eng.* **26**(10), 972–980.
- Jericevic, Z., Wiese, B., Bryan, J. & Smith, L.C. (1989) Validation of an imaging system: steps to evaluate and validate a microscope imaging system for quantitative studies. *Methods Cell. Biol.* **30**, 47–83.
- Kinney, P.D. & Talbot, R.J. (2006) Methods and Systems for In Situ Calibration of Imaging in Biological Analysis. Applera Corporation. 911.
- Kunz, L. & MacRobert, A.J. (2002) Intracellular photobleaching of 5,10,15,20-tetrakis(m-hydroxyphenyl) chlorin (foscan) exhibits a complex dependence on oxygen level and fluence rate. *Photochem. Photobiol.* **75**(1), 28–35.
- Lichtenstein, N., Geiger, B. & Kam, Z. (2003) Quantitative analysis of cytoskeletal organization by digital fluorescent microscopy. *Cytometry A* **54**(1), 8–18.
- Mullikin, J.C., van Vliet, L.J., Netten, H., Boddeke, E.R., Van Der Feltz, G. & Young, I.T. (1994) Methods for CCD camera characterization. *Proceedings of SPIE.* **2173**, pp. 73–84.
- Nicholson, W.L. (1978) Application of statistical methods in quantitative microscopy. *J. Microsc.* **113**(3), 223–239.
- Song, L., Hennink, E.J., Young, I.T. & Tanke, H.J. (1995) Photobleaching kinetics of fluorescein in quantitative fluorescence microscopy. *Biophys. J.* **68**(6), 2588–2600.
- Starosolski, R. (2005) Compressing images of sparse histograms. *SPIE Proceedings*. **5959**, pp. 209–217.
- Stelzer, E.H.K. (1998) Contrast, resolution, pixelation, dynamic range and signal to noise ratio: fundamental limits to resolution in fluorescence light microscopy. *J. Microsc.* **189**(1), 15–24.
- Sugiyama, Y., Kawabata, I., Sobue, K. & Okabe, S. (2005) Determination of absolute protein numbers in single synapses by a GFP-based calibration technique. *Nat. Methods* **2**(9), 677–684.
- Van Den Doel, L.R., Klein, A.D., Ellenberger, S.L., Netten, H., Boddeke, E.R., van Vliet, L.J. & Young, I.T. (1998) Quantitative evaluation of light microscopes based on image processing techniques. *Bioimaging* **6**, 138–149.
- Van Oostveldt, P., Verhaegen, F. & Messens, K. (1998) Heterogeneous photobleaching in confocal microscopy caused by differences in refractive index and excitation mode. *Cytometry* **32**, 137–146.
- Vermolen, B.J., Garini, Y., Mai, S., Mougey, V., Fest, T., Chuang, T.C., Chuang, A.Y., Wark, L. & Young, I.T. (2005) Characterizing the three-dimensional organization of telomeres. *Cytometry A* **67**(2), 144–50.
- Young, I.T. (1996) Quantitative Microscopy. *IEEE Eng. Med. Biol.* **15**(1), 59–66.
- Young, I.T., Garini, Y., Vermolen, B., Liqui Lung, G., Brouwer, G., Hendrichs, S., elMorabit, M., Spoelstra, J., Wilhelm, E. & Zaal, M. (2006) Absolute fluorescence calibration. *Proc. of SPIE.* **6088**, pp. 1–9.
- Young, P. (1998) Data-based mechanistic modeling. *Environ. Model. Soft.* **13**(2), 105–122.
- Young, P., Pedregal, D.J., Tych, W. (1999) Dynamic harmonic regression. *J. Forecast.* **18**, 169–394.
- Zucker, R.M. (2006a) Evaluation of confocal microscopy system performance. *Methods Mol. Biol.* **319**, 77–135.
- Zucker, R.M. (2006b) Quality assessment of confocal microscopy slide-based systems: Instability. *Cytometry A* **69A**(7), 677–690.

- Zucker, R.M. & Price, O. (2001a) Evaluation of confocal microscopy system performance. *Cytometry A* **44**(4), 273–94.
- Zucker, R.M. & Price, O.T. (2001b) Statistical evaluation of confocal microscopy images. *Cytometry A* **44**(4), 295–308.
- Zwier, J.M., van Rooij, G.J., Hofstraat, J.W., Brakenhoff, G.J. (2004) Image calibration in fluorescence microscopy. *J. Microsc.* **216**(1), 15–24.

Appendix

Block diagram of algorithm for calculation of significant intensity levels.

